Concepts for Experiments at Future Colliders I

PD Dr. Oliver Kortner

27.01.2025

Recapitulation of the previous lecture

Role of muons at hadron colliders

- Muons are the only charged primary collision products traversing the calorimeters.

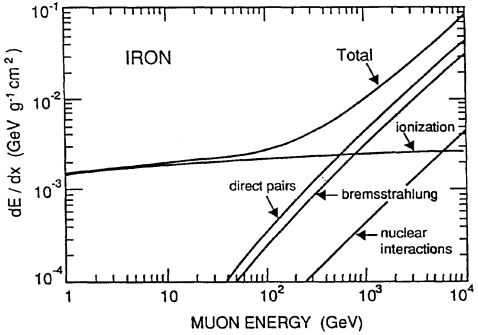

→ Clean signature of muonic final states.

- Example physics processes with muonic final states:
  - $H \to ZZ^* \to \mu\mu\ell\ell$,
  - $A \to \mu\mu$,
  - $Z' \to \mu\mu$.

- Good muon identification and reconstruction is crucial for physics at

Recapitulation of the previous lecture

Characteristic muon momentum spectra

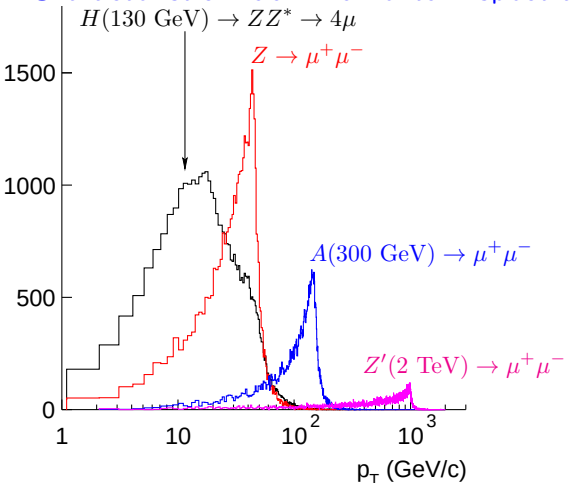

Need for efficient muon detection and identification over wide momentum range!

Muon identification tasks

Inclusive muon cross sections

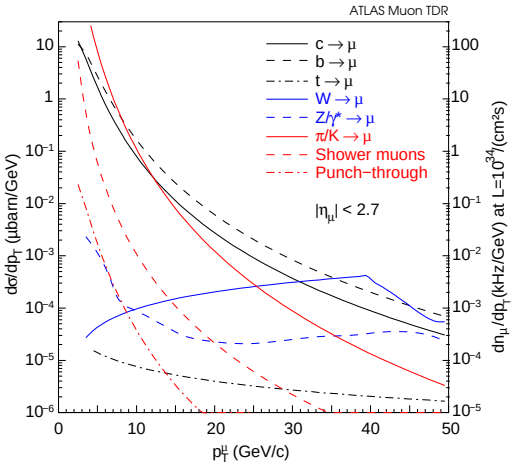

Muon identification tasks

- Identification of "prompt" muons from c, b, t, W, and Z/γ decays.
- Rejection of muon from π/K decays, shower muons, and hadronic punch-through.

Muon identification strategy

Muon identification concept

Goal	Solution
Minimization of hadronic punch-through	Muon system surrounding the calorimeters
Suppression of muons from π/K decays in flight	p_t measurement in the muon system with $\frac{\Delta p_t}{p_t} \lesssim 10\%$ + requirement of a well matching inner-detector track
Suppression of shower muons	As $\pi/K \to \mu$ + requirement of a small energy deposit in the calorimeters

The ATLAS and CMS Muon Systems

Recapitulation of the previous lecture

Limiting factors of the muon systems

Energy loss in the calorimeters:

- Energy loss ∼3 GeV with $\lesssim$20% fluctuation.
- Larger fluctuations can be measured by the calorimeters

→ Neglible influence on $\frac{\Delta p_t}{p_t}$ for $p_t \gtrsim 10$ GeV/c.

Multiple scattering (MS) in the calorimeters:

- Negligible for ATLAS: $\frac{\Delta p_t}{p_t}|_{MS} \sim 10^{-3}$.

Multiple scattering and bending power in the muon system:

- $\frac{\Delta p_t}{p_t} \propto \frac{\sqrt{\text{material in the muon system } [X_0]}}{\int B\, dl}$.

Resolution of the muon chambers:

- Spatial resolution σ of the muon chambers is the limiting factor for $\frac{\Delta p_t}{p_t}$ for high $p_t \sim 1$ TeV/c.
- $\frac{\Delta p_t}{p_t} \propto \sigma$ for $p_t \sim 1$ TeV/c.

The ATLAS and CMS Muon Systems

Two concepts for the muon system

ATLAS

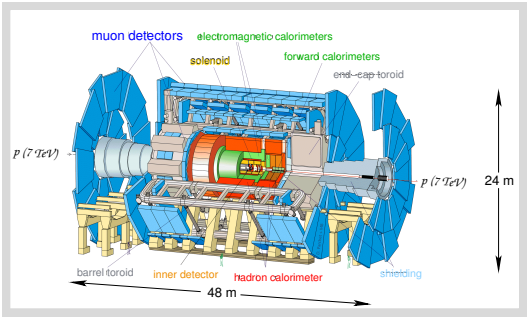

- Focus on stand-alone muon reconstruction.

→ Air-core toroid → minimization of multiple scattering.

CMS

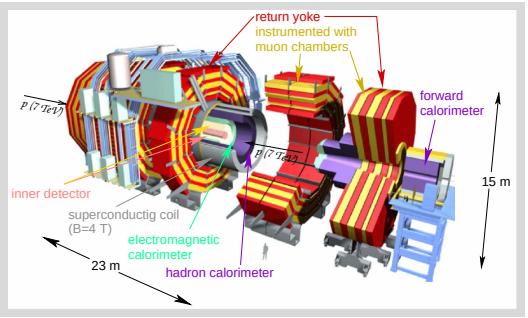

- Focus on high $\int B\,dl$ in the inner detector and compactness.
- Instrumented return yoke of the solenoid to achieve high bending power.

Recapitulation of the previous lecture

Magnets

ATLAS Air-Core Toroid

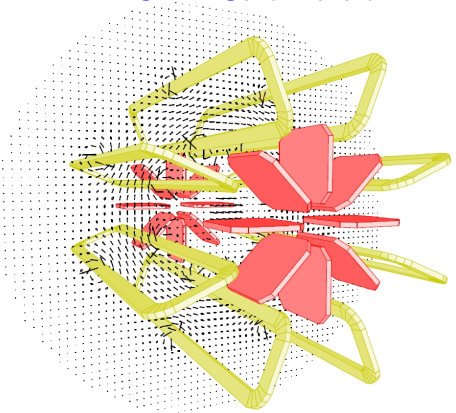

- No limitation of $\frac{\Delta p_t}{p_t}$ by MS.
- Accurate B-field measurement possible.
- Uniform $\frac{\Delta p_t}{p_t}$ independent of η.

Iron Return Yoke of CMS Solenoid

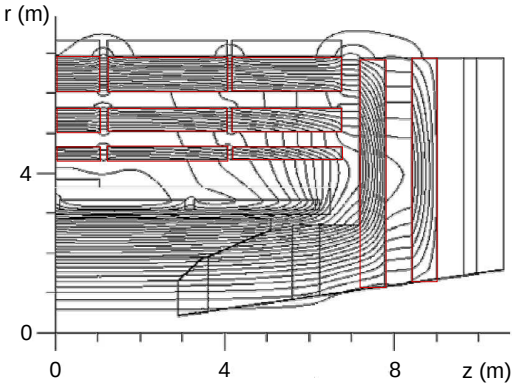

- Uniform B field in the barrel.
- High bending power.
- Limitation of $\frac{\Delta p_t}{p_t}$ by MS.
- η dependent $\frac{\Delta p_t}{p_t}$.

Comparison of the magnetic field integrals

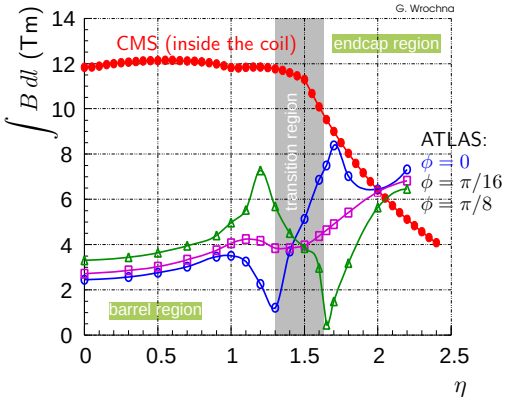

Barrel: $\approx 5\times$ higher bending power in CMS,
but $\approx 14\times$ larger multiple scattering.

$\rightarrow$ $\approx 3\times$ worse p_t resolution in CMS.

Endcap: similar bending powers,
$\approx 10\times$ large multiple scattering.

$\rightarrow$ $\approx 5\times$ worse p_t resolution in CMS.

Standalone transverse momentum resolution

ATLAS barrel standalone

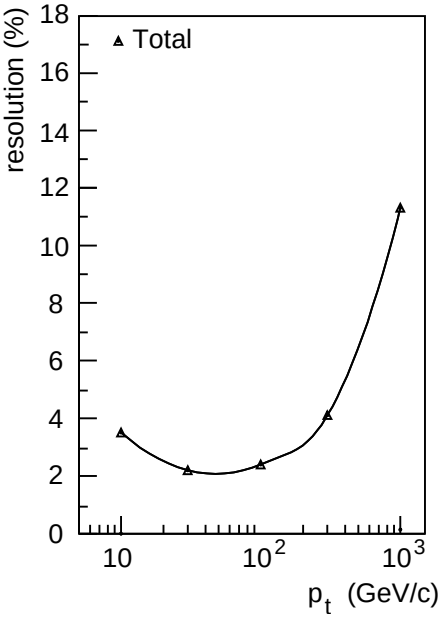

CMS barrel standalone

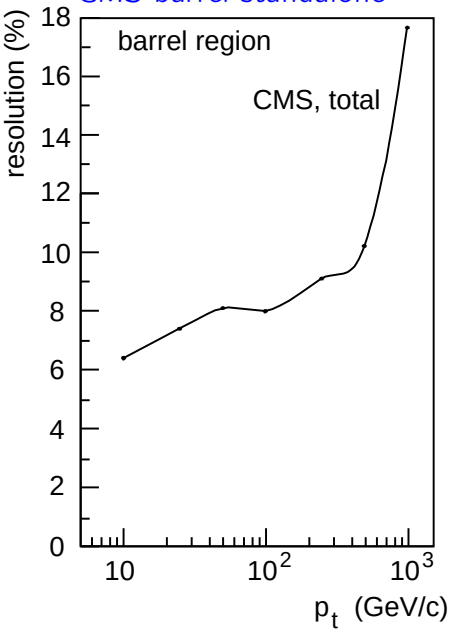

Recapitulation of the previous lecture

Standalone transverse momentum resolution

ATLAS barrel standalone

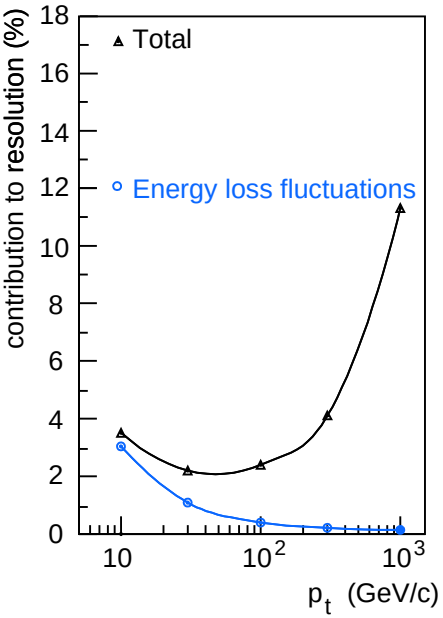

CMS barrel standalone

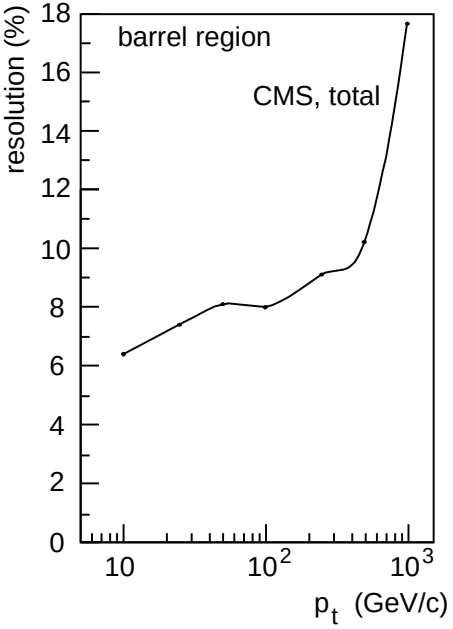

Recapitulation of the previous lecture

Standalone transverse momentum resolution

ATLAS barrel standalone

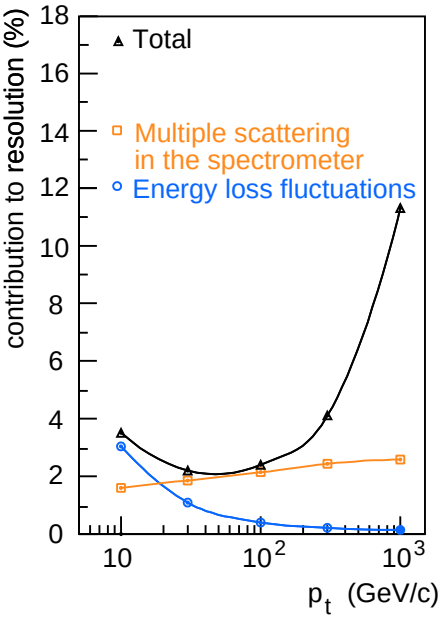

CMS barrel standalone

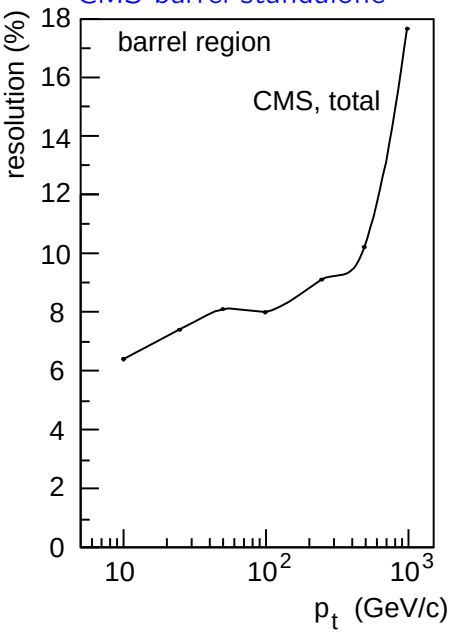

Recapitulation of the previous lecture

Standalone transverse momentum resolution

ATLAS barrel standalone

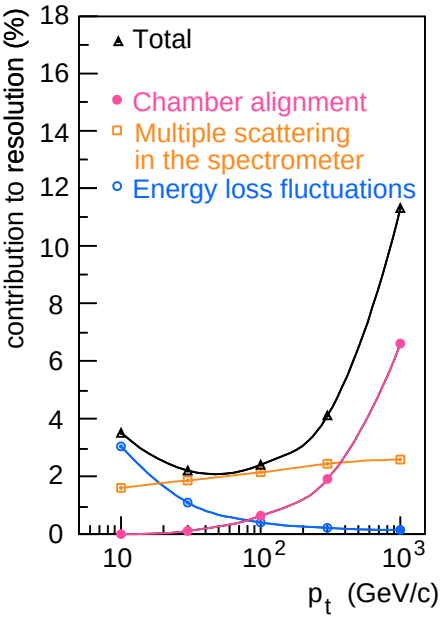

CMS barrel standalone

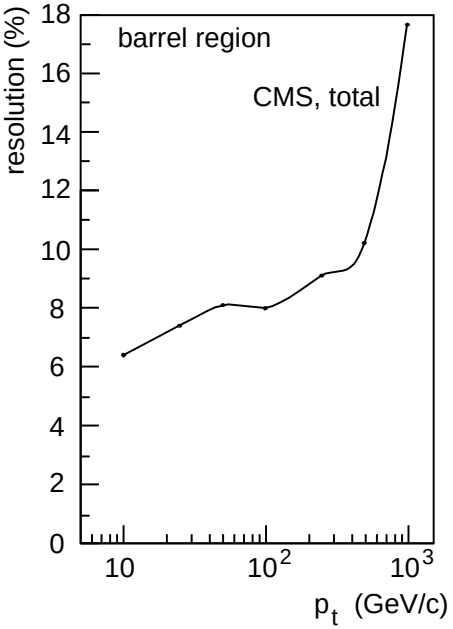

Recapitulation of the previous lecture

Standalone transverse momentum resolution

ATLAS barrel standalone

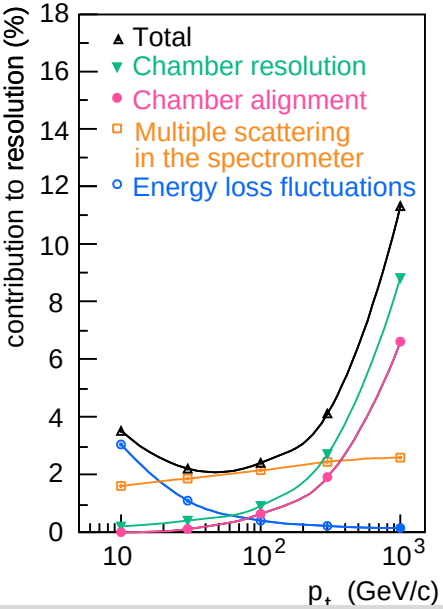

CMS barrel standalone

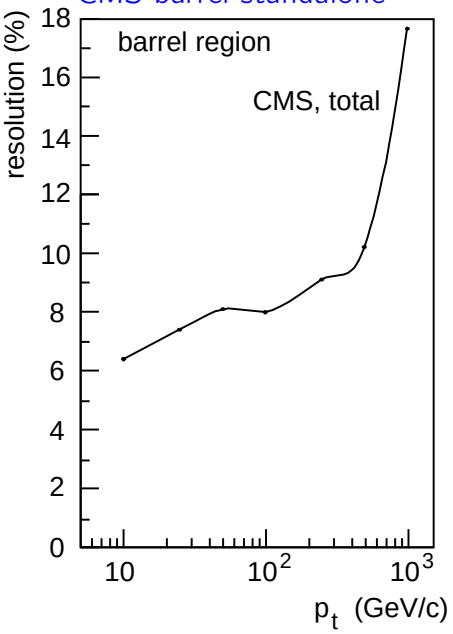

Recapitulation of the previous lecture

Standalone transverse momentum resolution

ATLAS barrel standalone

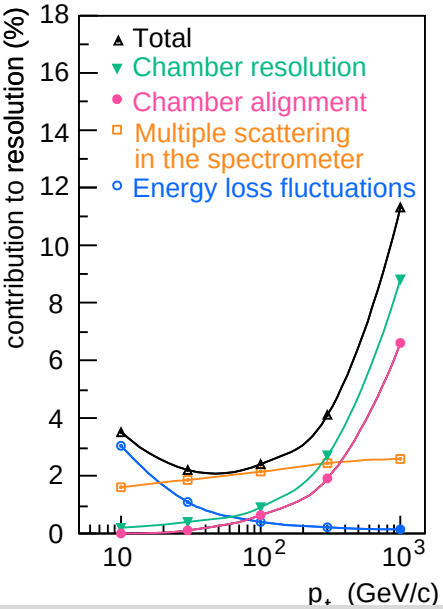

CMS barrel standalone

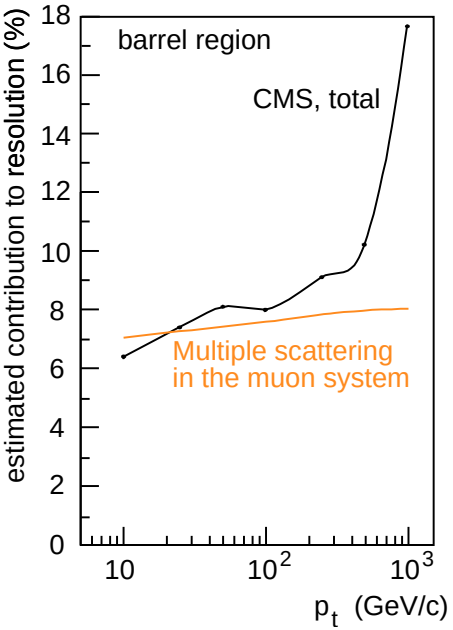

Recapitulation of the previous lecture

Standalone transverse momentum resolution

ATLAS barrel standalone

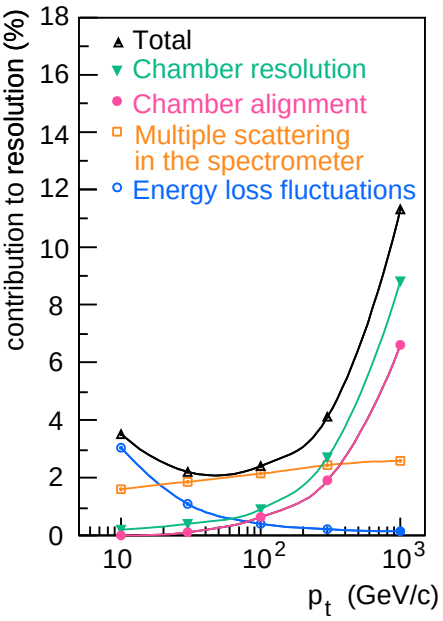

CMS barrel standalone

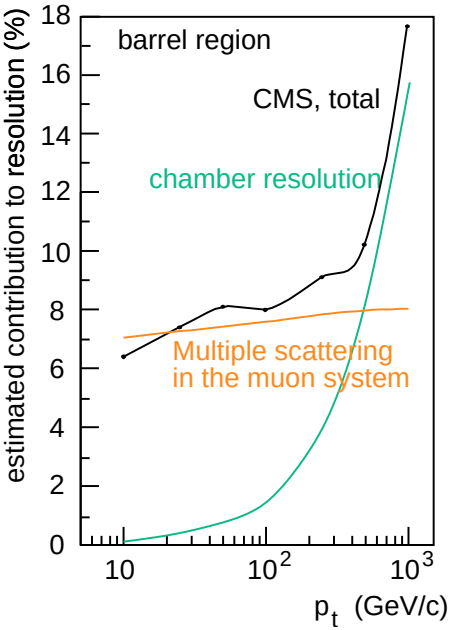

Recapitulation of the previous lecture

Combined transverse momentum resolution

Better resolution with muon systems and inner trackers

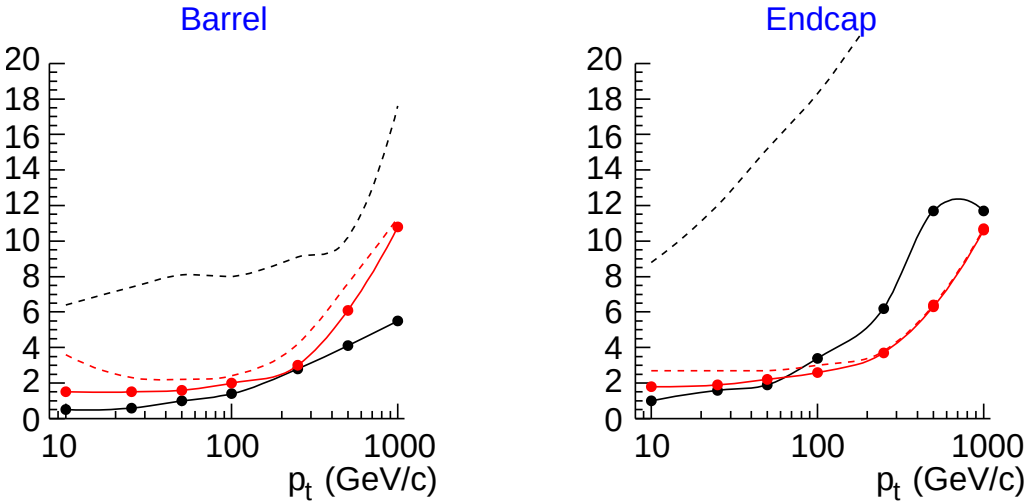

Better inner tracker resolution in CMS mainly due to higher B field

Advantages of a toroidal field

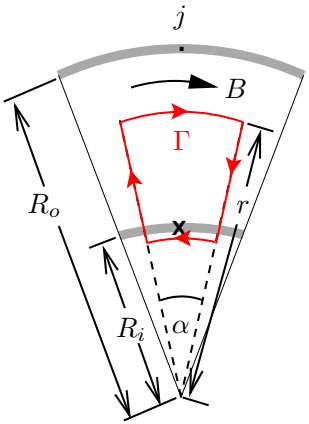

Ideal toroid

Ampère's law :

$$\oint_\Gamma \vec{B} \cdot d\vec{s} = B \cdot r \cdot \alpha = \mu_0 j \cdot R_i \cdot \alpha.$$

$$\Leftrightarrow B(r) = \frac{\mu_0 j R_i}{r} =: B_i \frac{R_i}{r}.$$

Advantages of a toroidal field

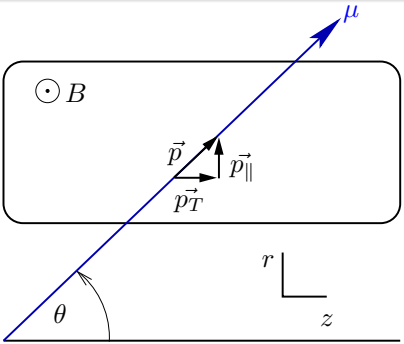

Field integral in a toroidal field

- Simplification: straight path for high p.

→ Trajectory

$$\vec{x}_\mu = \begin{pmatrix} x_0 \\ z_0 + r\tan\theta \\ r \end{pmatrix}.$$

$$d\vec{x}_\mu = \frac{d\vec{x}_\mu}{dr} \cdot dr = \begin{pmatrix} 0 \\ \tan\theta \\ 1 \end{pmatrix}.$$

$$|\vec{B} \times d\vec{x}_\mu| = \sqrt{1+\tan^2\theta}B(r)\,dr.$$

$$\int_{\mathcal{P}} B\,dl = \sqrt{1+\tan^2\theta}\int_{R_i}^{R_o} B_i\frac{R_i}{r}\,dr = \sqrt{1+\tan^2\theta}B_iR_i\ln\frac{R_o}{R_i}.$$

$$\alpha = \frac{q}{p_T}B_iR_i\ln\frac{R_o}{R_i}.$$

$$p = \sqrt{p_\parallel^2+p_T^2} = p_T\sqrt{1+\left(\frac{p_\parallel}{pT}\right)^2} = p_T\sqrt{1+\tan^2\theta}.$$

$\Rightarrow$ p_T resolution independent of θ (η)!

Reference detector for the CDR

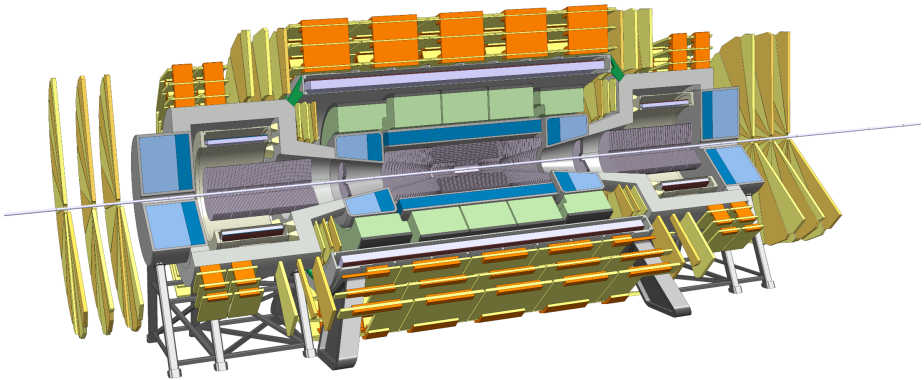

- 4 T 10 m solenoid + solenoids in the forward regions.
- Silicon semiconductor inner tracker.
- Liquid argon calorimeter.
- One muon chamber layer. Momentum measurement for the trigger using the muon's direction of flight in the muon system.

Instrumentation of the muon system

Boundary conditions

- Instrumentation of a large area (~ 10000 m^2) with position sensitive detectors.
- Detector requirements:
  - Fast response in order to be able to associate the detected muons to the pp collision in which they were created.
  - High spatial resolution in order to achieve the desired high momentum resolution.

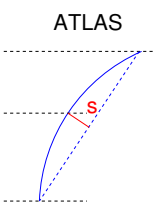

Measured quantity: Sagitta s.
Required accuracy: 50 μm.

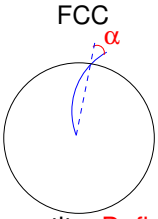

Measured quantity: Deflection angle α.
Required accuracy: 70 μrad.

- The muon detectors must be capable of an environment with high background radiation of neutrons and γs, which lead to count rates of up to ~ 10 kHz/cm^2.

Gaseous ionization detectors

- Only gaseous ionization detectors allow for a cost effective instrumentation of muon systems.

Explanation of the functioning principle using cylindrical tubes, filled with gas, as example

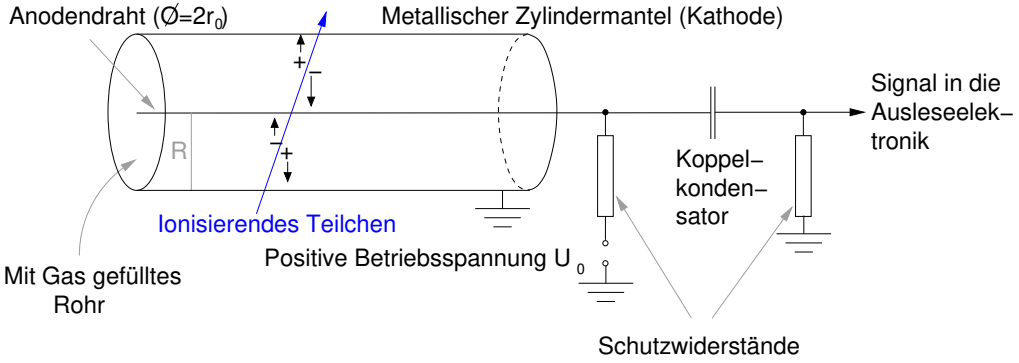

Radial electric field inside the tube: $E(r) = \frac{U_0}{\ln \frac{R}{r_0}} \frac{1}{r}$.

$\Rightarrow$ High field strength in the vicinity of the anode wire.

Signal strength as a function of U_0

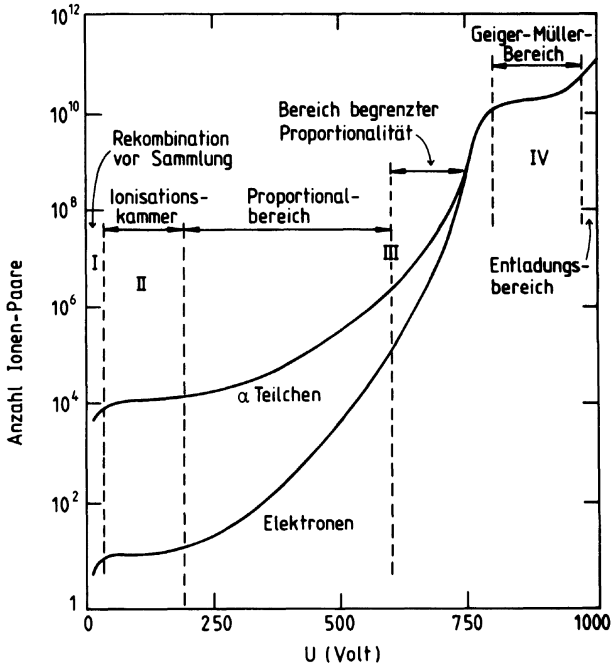

Ionization mechanism

Energy loss of charged particles by excitation and ionization of atoms.
X: Atom/molekule. p: Charged particle.

Excitation: $X + p \rightarrow X^* + p$. The reaction of X^* with other atoms/molecules can lead to ionization.

Ionization: $X + p \rightarrow X^+ + p + e^-$. The created charges X^+ and e^- are called primary ionization.

Average number of created electron ion pairs

Typical value: 1 elcktron ion pair per 30 eV energy loss.

Recombination and electron attachment

In order to get a signal in a tube, as many primary electrons must reach the anode wire. Ions created in the avalanche at the anode wire should reach the cathode. Two processes can lead to a loss of charge:

Recombination: $X^+ + e^- \rightarrow X + h\nu.$

$X^+ + Y^- \rightarrow XY + h\nu.$

Rekombination: $e^- + X \rightarrow X^- + h\nu.$

X: Atom with almost filled outer shell. $\rightarrow$ Positive electron affinity.

Examples: O_2, H_2O, CO_2, CCl_4, SF_6.

Noble gases have full outer shells. So they have negative electron affinity and are used in gaseous ionization detectors.

The motion of electrons and ions in the gas has two components: the thermal motion and the motion due to the presence of the electric field.

Thermal motion

- No preferred direction.
- $$v_{thermisch} = \sqrt{\frac{8k_BT}{\pi m}} \approx \begin{cases} 10^6 \text{ cm s}^{-1} \text{ for electrons} \\ 10^6 \text{ cm s}^{-1} \text{ for ions} \end{cases}$$

  at room temperature.
- Mean free path of electrons and ions between two collisions with gas molecules:

$$\lambda = \frac{1}{\sqrt{2}} \frac{k_BT}{\sigma_0 p}.$$

Motion under the influence of the electric field

t: Time passed since the last collision with a gas molecule.

$\vec{v}_0$: Velocity since the last collision.

Velocity at time t: $\vec{v}_0 + \frac{q}{m}\vec{E}t$s.

$$\begin{aligned} < \vec{v}_0 > &= 0. \\ < t > &= \text{mean time between two collisions } \tau. \\ \Rightarrow \qquad & \vec{u} = \frac{q\vec{E}}{m}\tau = \mu\vec{E}. \end{aligned}$$

$\vec{u}$ is called the drift velocity, μ the mobility.

For ions $u \ll v_{thermisch}$ such that $\tau = \frac{\lambda}{v_{thermal}}$, which leads to

$$\vec{u} = \frac{q}{4\sigma_0}\sqrt{\frac{\pi k_B T}{m}}\frac{E}{p}.$$

μ_{ions} is therefore independent of $\vec{E}$ and u_{ions} is proportional to $\frac{E}{p}$.
For electrons $u \sim v_{thermal}$ because of $m_e \ll m_{ion}$, and $\mu = \mu(E)$.

In the vicinity of the anode wire of a cylindrial tube, the electric field is to large that the primary electrons get accelerated to strongly to ionize gas atoms. An avalanche of electric charges is created.

λ: Mean free path of an electron up to the secondary ionization.

$\alpha := \frac{1}{\lambda}$: Probability for the ionization per traversed path (so-called Townsend coefficient).

n: Number of the electrons at point x.

Number of the electrons at point $x + dx$: $n + dn = n + n \cdot \alpha dx$, hence $\frac{dn}{dx} = n\alpha \Leftrightarrow n = n_0 \cdot \exp(\alpha x)$, where n_0 is the number of primary electrons.

Gas gain: $G := \frac{n(wire)}{n_0}$.

Muon drift tube chambers

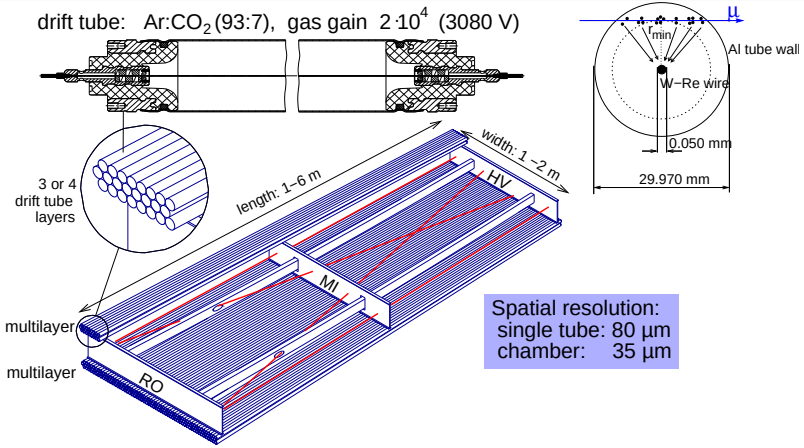

- MDT chambers with 30 mm and 15 mm tube diameter are used in the ATLAS muon spectrometer.
- MDT chambers with 15 mm diameter are part of the conceptual design of the muon system of the FCC-hh detector.
- Occupancy of these detectors at 10 kHz background count rate: 10 kHz cm^{-2}·200 ns=0,2% cm^{-2}=30% for 1 m tube length.

Resistive-Plate Chambers (RPCs)

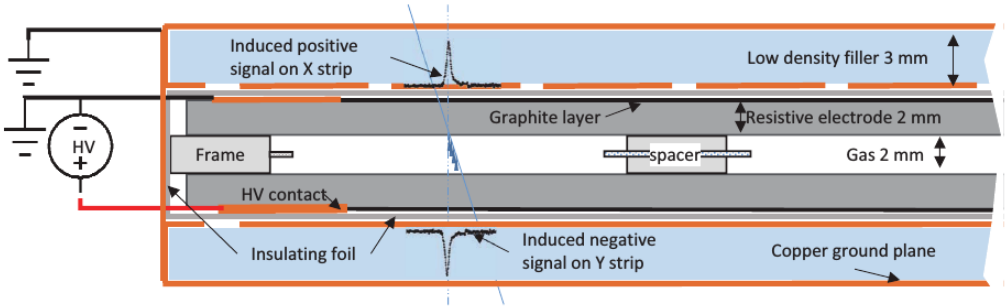

- Constant electric field inside the gas volume.

⇒ Avalanche creation everywhere in the gas volume along the trajectory of the ionizing particle. Fast reponse (~ 1 ns. High temporal resolution: ~ 0.5 ns.

- In order to prevent a short between the electrodes and to terminate the avalanche creation, electrodes with high resistivity are used.

Micropattern gaseous ionization detectors

- The charge particle detection efficiency of a detector under high particle background is given/determined by the size of its active "space-time" area, i.e. its spatial granularity and its dead time.
- Micropattern gaseous ionization detectors are fast gaseous ionization detectors with high spatial granularity for the operation in high background environments.
- Most prominent examples: GEMs, MicroMegas.

Gas Electron Multiplier (GEM)

- The heart of a GEM is a thin, metal-clad polymer foil, chemically pierced by a high density of holes (typically 50 to 00 per mm^2.
  On application of a difference of potential between the two electrodes, electrons released by radiation in the gas on one side of the structure drift into the holes, multiply and transfer to a collection region.

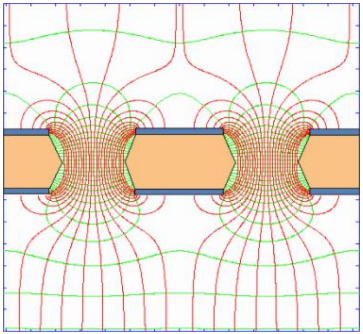

Field lines and equipotentials in the GEM holes on application of a voltage between the two metal sides. A drift (top) and transfer field (bottom) transport ionization electrons into and out of the holes.

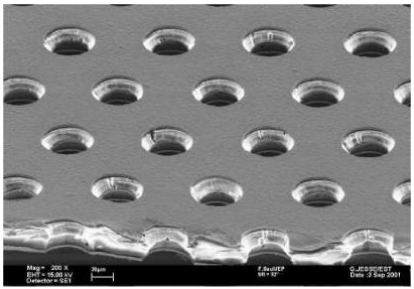

Close view of a GEM electrode, etched on a metal-clad, 50 μm thick polymer foil. The hole's diameter and distance are 70 μm and 140 μm.

Single and multiple GEMs

Schematics of a single GEM detector. Electrons released by ionization in the top gas volume drift and multiply in the holes; the charge is collected on the anode, with 1-D or 2-D projective strips, pads or other patterns.

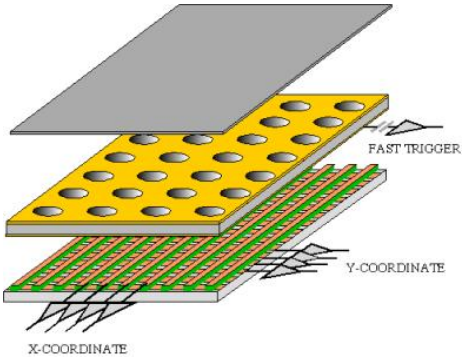

A triple-GEM detector: gain sharing between the foils improves the reliability of operation at high gains.

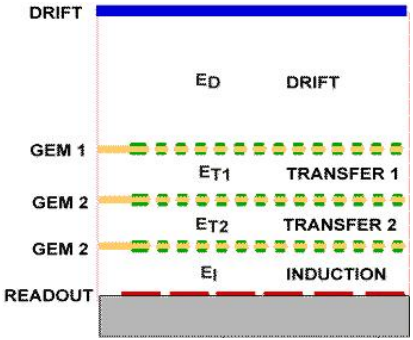

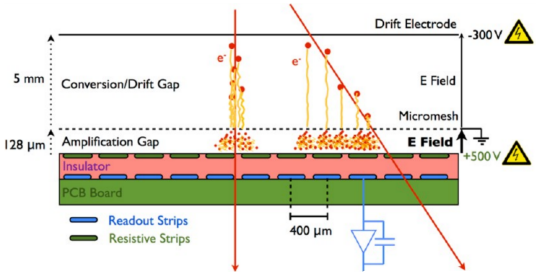

- A MicroMegas can be considered as an RPC with an additional ionization and drift region.
- Advantage of the additional ionization region: higher primary charge than in an RPC.
- Disadvantage of the additional ionization region: A MicroMegas is slower than an RPC.

Time-Projection Chamber

- Time-projection chambers were developed in the 1980s to allow for charge particle detections with a very small amount of material along the track.

Leo 1993

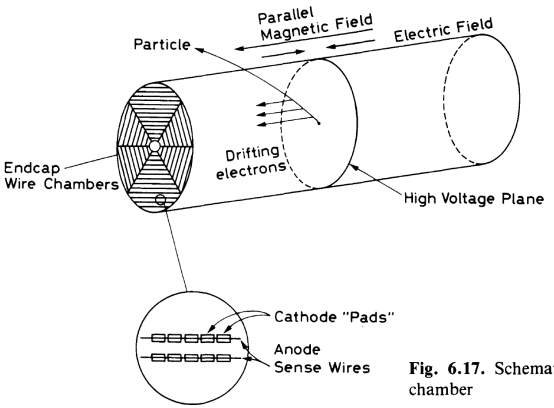

Fig. 6.17. Schematic diagram of a time projection chamber

- Modern TPCs use different detectors on the end caps, e.g. GEMs.
- Problem at the FCC-ee: Magnetic field must not exceed 2 T in order not to spoil the $e^{\pm}$ beams. This leads to a reduced spatial resolution.